Mon. Not. R. Astron. Soc. **000**, 1–10 (2012) Printed 7 August 2012 (MN LATEX style file v2.2)

VLA imaging of ^{12}CO $J=1-0$ and free-free emission in lensed submillimetre galaxies

A. P. Thomson,[1⋆] R. J. Ivison,[1,2] Ian Smail,[3] A. M. Swinbank,[3] A. Weiss,[4] J.-P. Kneib,[5] P. P. Papadopoulos,[4] A. J. Baker,[6] C. E. Sharon[6] and G. A. van Moorsel[7]

[1] *Institute for Astronomy, University of Edinburgh, Blackford Hill, Edinburgh EH9 3HJ*
[2] *UK Astronomy Technology Centre, Science and Technology Facilities Council, Royal Observatory, Blackford Hill, Edinburgh EH9 3HJ*
[3] *Institute for Computational Cosmology, Durham University, South Road, Durham DH1 3LE*
[4] *Max-Planck-Institut für Radioastronomie, Auf dem Hügel 69, 53121, Bonn, Germany*
[5] *Laboratoire d'Astrophysique de Marseille, CNRS-Université Aix-Marseille, 13388 Marseille Cedex 13, France*
[6] *Department of Physics and Astronomy, Rutgers, The State of New Jersey, 136 Frelinghuysen Road, Piscataway, NJ 08854-8019, USA*
[7] *National Radio Astronomy Observatory, 1003 Lopezville Road, Socorro, NM 87801, USA*

Accepted 2012 June 24. Received 2012 June 22; in original form in 2012 May 22

ABSTRACT

We present a study using the Karl G. Jansky Very Large Array (VLA) of ^{12}CO $J=1$–0 emission in three strongly lensed submillimetre-selected galaxies (SMM J16359, SMM J14009 and SMM J02399) at $z = 2.5$–2.9. These galaxies span $L_{\rm IR} = 10^{11-13}\,{\rm L}_\odot$, offering an opportunity to compare the interstellar medium of LIRGs and ULIRGs at high redshift. We estimate molecular gas masses in the range $2-40\times10^9\,{\rm M}_\odot$ using a method that assumes canonical underlying brightness temperature ($T_{\rm b}$) ratios for star-forming and non-star-forming gas phases and a maximal star-formation efficiency. A more simplistic method – using $X_{\rm CO} = 0.8$ and the measured $T_{\rm b}$ ratios – yields gas masses twice as high. In SMM J14009 we find $L'_{\rm CO3-2}/L'_{\rm CO1-0} = 0.95\pm0.12$, indicative of warm, star-forming gas, possibly influenced by the central active galactic nucleus (AGN). We set a gas mass limit of $3\sigma < 6\times10^8\,{\rm M}_\odot$ for the Lyman-break galaxy, A2218 #384, located in the same field as SMM J16359 at $z = 2.515$. Finally, we use the rest-frame ∼115-GHz free-free flux densities for SMM J14009 and SMM J02399 – measurements tied directly to the photoionisation rate of massive stars, and made possible by VLA's bandwidth – to estimate star-formation rates (SFRs) of 400–600 ${\rm M}_\odot\,{\rm yr}^{-1}$, and to estimate the fraction of $L_{\rm IR}$ due to AGN.

Key words: galaxies: active — galaxies: high-redshift — galaxies: starburst — submillimetre — ISM: molecules — galaxies: ISM

1 INTRODUCTION

Observations of the interstellar medium (ISM) in high-redshift galaxies can provide insight into the process of star formation within these systems. Although the bulk of the molecular gas – the fuel for future star formation – is in the form of H_2, its lack of a net dipole moment prevents H_2 from radiating strongly under normal ISM conditions. However, this gas can be detected indirectly due to the collisional excitation it induces in heteronuclear and near-ubiquitous ^{12}CO – the second most abundant molecule in the ISM – which emits electromagnetic radiation when its angular momentum quantum number changes by $\hbar$. The low dipole moment of ^{12}CO enables its excitation in regions of low density, $n_{\rm crit} \geqslant 10^2\,{\rm cm}^{-3}$, making it an ideal tracer of the bulk of the molecular gas reservoir, allowing us to determine its properties in a manner unbiased by the patchy dust extinction which can lead to misleading views of velocity fields and galaxy morphologies via optical/near-infrared studies.

Since the earliest detections of ^{12}CO in high-redshift galaxies (e.g. Brown & Vanden Bout 1991; Solomon et al. 1992), much effort has been put into discerning the mass, extent and physical properties of the H_2 gas in galaxies across cosmic time; this offers a snapshot of their evolutionary state and narrows down the possibilities for their likely descendents. Until now, available technology has limited the study of ^{12}CO at high redshift to relatively bright, mid-J lines (^{12}CO $J = 3-2$ and above), which are shifted into broad, clean atmospheric windows such as that at 3 mm. The excitation requirements of these

⋆ E-mail: at@roe.ac.uk

lines render such observations insensitive to any cool, extended gas component, wherein much of the gas is routinely found (e.g. Papadopoulos & Seaquist 1999; Weiß et al. 2005; Bothwell et al. 2012). For local galaxies the intrinsically fainter $J = 1-0$ transition occupies the 3-mm atmospheric window and mid-J lines are more difficult to study, requiring high-frequency receivers and excellent atmospheric conditions. Efforts to conduct comparative studies at low and high redshift have therefore been few and far between, and the relationship between high-redshift galaxies and their myriad possible present-day descendants is not well understood.

Gravitational amplification – either by chance, line-of-sight foreground galaxies (e.g. Rowan-Robinson et al. 1991; Graham & Liu 1995; Negrello et al. 2010) or by deliberate exploitation of massive, foreground clusters (e.g. Kneib 2010) – has provided samples that have formed the basis for much of our understanding of the distant starbursts that dominate the cosmic far-infrared/submm background. Usually buried in the confusion noise, these faint galaxies become relatively easy to detect and spatially resolve by virtue of the magnification they experience. Such an approach led to the discovery of submillimetre-selected galaxies (SMGs – Smail et al. 1997), to the relatively straightforward identification of their radio and optical counterparts, acquisition of their redshifts (e.g. Ivison et al. 1998) and their detection in mid-J ^{12}CO (e.g. Frayer et al. 1998). The redshift distribution of SMGs is broad, centred at $z \sim 2.3$ (Chapman et al. 2005), and their inferred stellar masses ($\sim 10^{10-11}$ M$_\odot$) and star-formation rates (SFRs; $\sim 10^3$ M$_\odot$ yr^{-1}) make them among the most massive and active galaxies at this epoch (e.g. Hainline et al. 2011).

Here, we follow this familiar pattern. We exploit the recent upgrade to the National Radio Astronomy Observatory's (NRAO's[1]) Karl G. Jansky Very Large Array (VLA), which includes the provision of Ka-band receivers (26.5–40 GHz), to study the redshifted ^{12}CO $J = 1-0$ emission from three lensed SMGs: (i) SMM J14009+0252 lying at $z = 2.9344$ (Ivison et al. 2000; Weiß et al. 2009), lensed by Abell 1835 and one of the brightest SMGs detected in the SCUBA Cluster Lens Survey (SCLS; Smail et al. 2002) (ii) SMM J16359+6612, a bright SMG a $z = 2.5168$ (Kneib et al. 2004, 2005) and lensed into three images by the Abell 2218 cluster, and (iii) SMM J02399–0136 at $z = 2.808$ (Ivison et al. 1998), the first SCUBA galaxy and the brightest of the SCLS galaxies, lensed by Abell 370. We also search for ^{12}CO $J = 1-0$ emission in (iv) the Lyman-break galaxy (LBG) A 2218 #284, located 22.1 arcsec from the centre of the lensing cluster in the same field as SMM J16359 (Ebbels et al. 1996).

The optical spectrum of SMM J02399, coupled with its extreme luminosity and emission-line widths (FWZI $\sim 1,000$ km s^{-1}) have long been cited as evidence that this source contains a type-2 active galactic nucleus (AGN; Ivison et al. 1998). SMM J14009 too has long been suspected to host a dust-enshrouded AGN on the basis of the strength of its radio emission ($S_{1.4\,\mathrm{GHz}} = 529 \pm 30\mu$Jy) and compactness (Ivison et al. 2000, Biggs et al. *in prep.*).

Due to the effects of lensing, we benefit from a boost in flux density and apparent size of our targets, surface brightness being conserved. Excellent lens models exist for Abell 370, 1835 and 2218 and multi-wavelength imaging has constrained the ages, stellar masses and SFRs of our targets, as well as the mass of warm, star-forming gas as traced by, e.g., ^{12}CO $J = 3-2$. Observations of another SMG lensed by A 1835, SMM J14011+0252 at $z = 2.5652$, will be discussed by Sharon et al. *in prep.*

Throughout the paper we use a cosmology with $H_0 = 71$ km s^{-1} Mpc^{-1}, $\Omega_\mathrm{m} = 0.27$, $\Omega_\Lambda = 0.73$. which gives an average angular scale of 8.1 kpc arcsec^{-1} for our sample.

2 OBSERVATIONS AND DATA REDUCTION

2.1 VLA observations

Observations of SMM J14009 and SMM J16359 were carried out in blocks of 2–4 hr during excellent weather conditions between 2010 April and 2011 January (Project IDs: AI139 and AI142). Over this Open Shared Risk Observing period the available bandwidth from the new Wideband Interferometric Digital ARchitecture (WIDAR) correlator consisted of two sub-band pairs, each with 64×2-MHz dual-polarisation channels, and the number of useful Ka receivers roughly doubled, from ~ 10 to ~ 20. Due to the different redshifts of the targets, different tuning strategies had to be employed in each case: for SMM J16359 we used both sub-band pairs with the frequency of the redshifted ^{12}CO $J = 1-0$ line ($\nu_\mathrm{rest} = 115.27120256$ GHz – Morton & Noreau 1994) placed in channel 40 of the lower sub-band and a 10-channel overlap between the two sub-bands to mitigate the effects of noise in the edge channels. This configuration gave velocity coverage and resolution of $\sim$2,000 km s^{-1} and $\sim$18 km s^{-1}, respectively. For the higher-redshift SMM J14009, the redshifted emission was accessible to only one of the two sub-bands and the line was placed in its centre providing $\sim$1,300 km s^{-1} coverage, the other sub-band being tuned to $\nu_\mathrm{obs} = 32.4$ GHz in order to constrain the $\sim$130-GHz radio continuum.

By the time SMM J02399 was observed during 2011 September through November (Project ID: AT400), the OSRO capabilities had been upgraded to include two independently tunable output pairs of eight sub-bands each, with 128×1-MHz dual-polarisation channels per sub-band, giving a total available bandwidth of 2,048 MHz. Again, however, the redshift of SMM J02399 could be reached by only the BD output pair, giving $\sim$20,000 km s^{-1} of coverage and $\sim$10 km s^{-1} resolution. The 8 sub-bands of output pair AC were tuned continuously at the lowest possible central frequency, 32.52 GHz, to constrain the radio continuum emission from this source.

For SMM J16359 we obtained approximately 19 and 14 hr of useful data in the VLA's D and C configurations; for the equatorial target SMMJ 14009 we employed the DnC and CnB configurations (with their longer northern arms), acquiring 8 and 16 hr, respectively. 10 hr of on-source D configuration observations were performed for SMM J02399, though an unfortunate technical problem with the correlator resulted in only 1/3 of the observed data being recorded.

Antenna pointing was checked using the C-band receivers every 60–90 min, and immediately prior to scans of the flux calibrator (3C 286 for SMM J14009

[1] NRAO is operated by Associated Universities Inc., under a cooperative agreement with the National Science Foundation.

Table 1. VLA sample and observing log.

Target	Magnifi-ication	z	$\Delta\nu_{\rm obs}$ (GHz)	Configu-ration	Observing dates	Reference
SMM J14009	1.5	2.9344	29.23	DnC	Sep 25, 29, 30 (2010),	Weiß et al. (2009)
			–29.36	CnB	Jan 21, 24, 26, 27 (2011)	
SMM J16359	14, 22, 9[a]	2.5168	32.69	D	Apr 12, 14, 20, May 05, 20 (2010),	Kneib et al. (2004)
			–32.93	C	Dec 31, Jan 04, 06, 10, 11 (2011)	
SMM J02399	2.45	2.808	29.73	D	Sep 27, Oct 26 ×2,	Genzel et al. (2003)
			30.69		Nov 01 ×2 (2011)	

Note: [a]Images A, B, C, respectively.

and SMM J16359; 3C 48 for SMM J02399). We tracked amplitude and phase with brief scans of J1642+6856 (for SMM J16359), J1354−0206 (for SMM J14009) and J0239−0234 (for SMM J02399), every 5 min. These data were also used to determine the bandpass.

Data were flagged, calibrated and imaged using standard $\mathcal{AIPS}$ procedures, as outlined by Ivison et al. (2011).

We constructed data cubes for each source using the CLEAN algorithm with 6-MHz ($\sim$ 50-km s^{-1}) resolution by binning the native VLA channels to boost signal-to-noise. We used natural weighting and Gaussian uv tapers to check for any flux which may have been resolved out in the high-resolution images but found no evidence for significant missing flux in any of our sources. The resulting synthesised beam sizes are 0.88×0.72 arcsec^2 with position angles (PAs) 125° for SMM J14009, 1.07×0.72 arcsec^2 at PA 22° for SMM J16359 and 3.08×2.56 arcsec^2 at PA 160° for SMM J02399; the integrated maps (Fig. 1) reach down to a noise levels of 20, 11 and 20 μJy beam^{-1}, respectively.

Spectra (see Fig. 2) were extracted from the data cubes with the $\mathcal{AIPS}$ task, ISPEC, which sums the flux density within a box around the source for each plane in the cube. Error spectra were produced by extracting five off-source spectra and calculating the standard deviations among these five sky spectra for each spectral channel. The mean noise values per spectral channel for SMM J14009, SMM J16359 and SMM J02399 were 0.09, 0.17 and 0.13 mJy beam^{-1}, respectively.

Line fluxes are measured by integrating the emission spectra across the width of each ^{12}CO line and then checked via the equivalent integrated image. In determining both the observational and derived source properties, we treat the three images of SMM J16359 as individual sources and then co-add the results to derive magnification-weighted averages where physically appropriate.

2.2 Infrared luminosities

Throughout the paper, we make reference to infrared properties of our sources, including calculations of the gas masses and SFR derived from rest-frame 8–1,000 μm luminosities, $L_{\rm IR}$. Here, we present the measurements used to derive these quantities.

We use archival data from *Herschel* (Pilbratt et al. 2010) to measure $S_{250\mu m}$, $S_{350\mu m}$ and $S_{500\mu m}$, together with published SCUBA flux densities at 750, 850 and 1350 μm. We then exploit the SED library of Chary & Elbaz (2001, hereafter CE01) in order to determine $L_{\rm IR}$ for each galaxy.

For SMM J02399 we use the mid-IR spectrum of Lutz et al. (2005), with data covering $\lambda_{\rm obs} \geqslant 750\mu$m taken from Ivison et al. (1998). In Fig. 3 we see the excellent agreement between the data and the best-fit SED template. The derived value of $L_{\rm IR} = (80.7 \pm 8.1) \times 10^{11}$ L$_\odot$ is 30 per cent lower than the value reported in Ivison et al. (1998).

For SMM J16359 we use published flux densities for the three images at 24 and 70 μm from Kneib et al. (2004). The three images are resolved by *Herschel* up to 350 μm but become blended at longer wavelengths. Where the three images are blended, we divide up the observed flux in proportion to the known magnification factors. We derive an estimate of $L_{\rm IR}$ for each of the three images of this source and combine our three estimates to derive the magnification-weighted mean $L_{\rm IR} = (6.4 \pm 1.0) \times 10^{11}$ L$_\odot$. This value is consistent with the results of Finkelstein et al. (2011), who determined $L_{\rm IR} = 7.0 \times 10^{11}$ L$_\odot$ (for image B) using a similar SED-fitting method.

Similarly, for SMM J14009 we rely on the 24-μm measurement from Hempel et al. (2008) to supplement the archival *Herschel* and SCUBA data, and compute a lensing-corrected $L_{\rm IR} = (160 \pm 24) \times 10^{11}$ L$_\odot$.

The best-fit CE01 SEDs for each galaxy are shown with the corresponding photometry in Fig. 3.

2.3 Radio continuum data

The VLA tuning strategies employed to observe ^{12}CO $J = 1-0$ in for SMM J14009 and SMM J02399 enabled us to obtain detections of the $\sim$ 115-GHz continuum emission from these galaxies. These data were reduced in parallel with and according to the same recipe as the ^{12}CO spectral-line data. We do not have continuum data at this frequency for SMM J16359, owing to the different tuning strategy employed at the VLA for this source. We detect continuum flux densities of $S_{32\,\rm GHz} = 57 \pm 25\,\mu$Jy for SMM J02399 and $S_{32\,\rm GHz} = 42 \pm 20\,\mu$Jy for SMM J14009. 1.4-GHz flux densities of $S_{1.4\,\rm GHz} = 526 \pm 50$ and $529 \pm 30\,\mu$Jy were determined in Ivison et al. (1998) and Ivison et al. (2000) for SMM J02399 and SMM J14009, respectively. The VLA science archive was queried for continuum data at 5- and 8-GHz as well, with flux densities reported in Table. 4. The radio continuum data are plotted with the IR SEDs in Fig. 3.

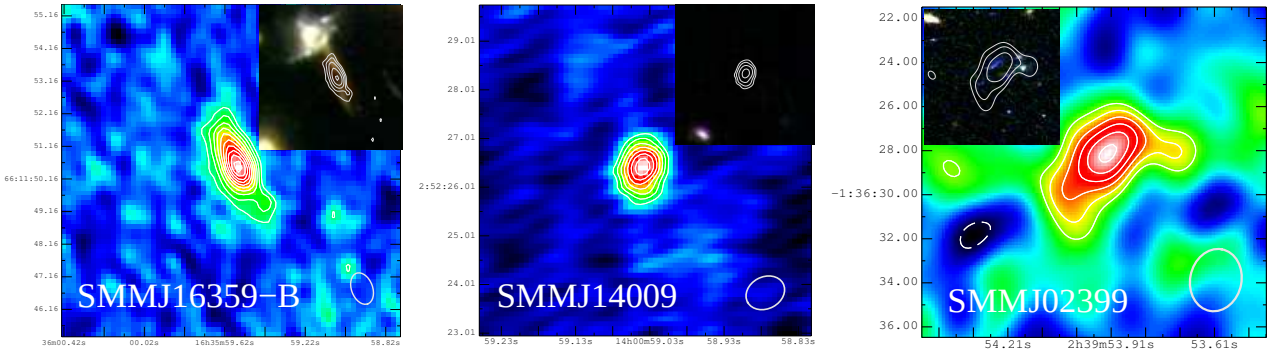

Figure 1. Integrated ^{12}CO $J = 1-0$ maps of our three targets, SMM J16359 (10 arcsec/side), SMM J14009 (10 arcsec/side) and SMM J02399 (15 arcsec/side). For SMM J16359 – a triply imaged source – we show only the brightest image, SMM J16359-B as defined by Kneib et al. (2004). *Main images:* ^{12}CO $J=1-0$ contours spaced at -3, 3, 4, 5...$\times\sigma$, set on top of colour representations of the same data. The VLA beam used to produce each map is shown in the bottom-right corner. *Insets:* ^{12}CO $J=1-0$ contours spaced at -3, 3, $\sqrt{2}\times3...\times\sigma$ and in steps of $\sqrt{2}\times\sigma$ thereafter, set on top of three-colour *HST* images of the same field of view, in order to explore the relationship between the SMG and any optical counterpart there may be. For SMM J14009 we detect no optical counterpart to the ^{12}CO emission.

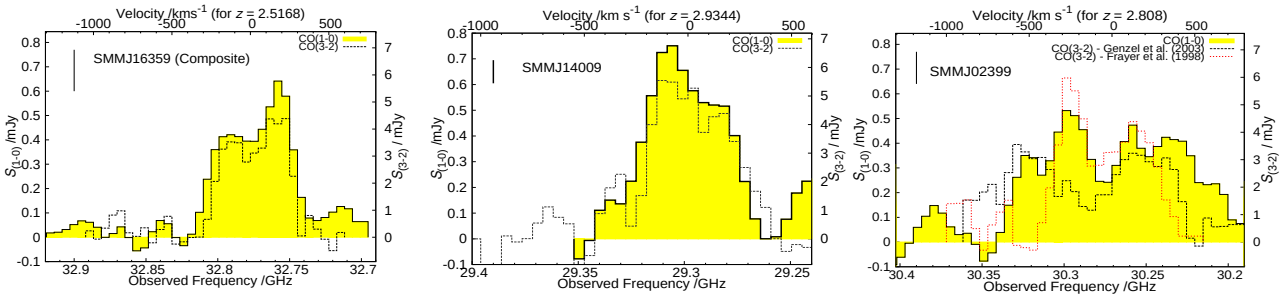

Figure 2. ^{12}CO $J=1-0$ spectra (yellow histograms) and reference $J=3-2$ spectra (dotted lines) for our three targets. The left-hand scale represents $J=1-0$ flux density, and the right-hand side shows the corresponding $J=3$–2 flux density, scaled by 9^{-1} so as to be on the same Rayleigh-Jeans $T_{\rm b}$ scale. The zero-LSR redshifts used to determine the relative velocities for each source are quoted in the figure, and typical error bars are shown in the top-left-hand corner of each plot. The spectrum shown for SMM J16359 is the magnification-weighted mean of the spectra of the three images of this source, SMM J16359-A, -B and -C as defined in Kneib et al. (2004).

3 ANALYSIS AND RESULTS

3.1 ^{12}CO morphologies and spectra

We summarise the source properties in Table 2. All sources are detected in ^{12}CO $J=1-0$ with signal-to-noise of 13 for SMM J16359-B (the brightest of three images of this multiply-lensed source), 17 for SMM J14009 and 7.5 for SMM J02399. The flux-weighted ^{12}CO $J=1-0$ redshifts – summarised in Table 2 – are derived by fitting a single Gaussian component to each ^{12}CO $J=1-0$ spectrum and are consistent with the reference ^{12}CO $J=3-2$ redshifts to four significant figures. The spectrum shown for SMM J16359 is a magnification-weighted average of the spectra from each image of this source. The uncertainties in the spectral fits translate to velocity uncertainties that are typically of order $\Delta V = 10$–$15\,{\rm km\,s^{-1}}$, except in the case of SMM J02399 where the comparatively low signal-to-noise hampers our ability to constrain $z_{\rm CO}$ and results in $\Delta V \sim 50\,{\rm km\,s^{-1}}$. For each source we see broad lines with full width at zero intensity (FWZI) of $\sim$500–1,000 $\rm km\,s^{-1}$.

We compare the line profiles and maps between $J=1-0$ and $J=3-2$ observations. The astrometry is consistent. For SMM J16359 and SMM J14009 we see good agreement between the low-J and mid-J ^{12}CO line profiles. In the former, we detect double-peaked $J=1-0$ line profiles for each of the three images, separated by $\sim300\,{\rm km\,s^{-1}}$, as did Kneib et al. (2005) in their study of the $J=3-2$ emission. SMM J02399 displays a significant offset in velocity between the measured $J=1-0$ emission and the $J=3-2$ spectrum of Genzel et al. (2003), $\sim100\,{\rm km\,s^{-1}}$, roughly twice that which could be ascribed to uncertainties in the Gaussian fits. However, the $J=1-0$ and $J=3-2$-derived redshifts are consistent to four significant figures ($z=2.808$). It is difficult to envisage any plausible physical origin for these offsets: in an effort to track down any instrumental contribution to the frequency offsets, continuous-wave tones were injected into the Ka-band receivers at frequencies close to those used for the science observations, but no offsets were observed between the input and observed tones (Emmanuel Momjian, private communication).

We find a weighted mean velocity width ratio of $\sigma_{(1-0)/(3-2)} = 1.3\pm0.1$ for the three images of SMM J16359, consistent with the findings of Ivison et al. (2011) for a sample of four unlensed SMGs. For the two more AGN-like

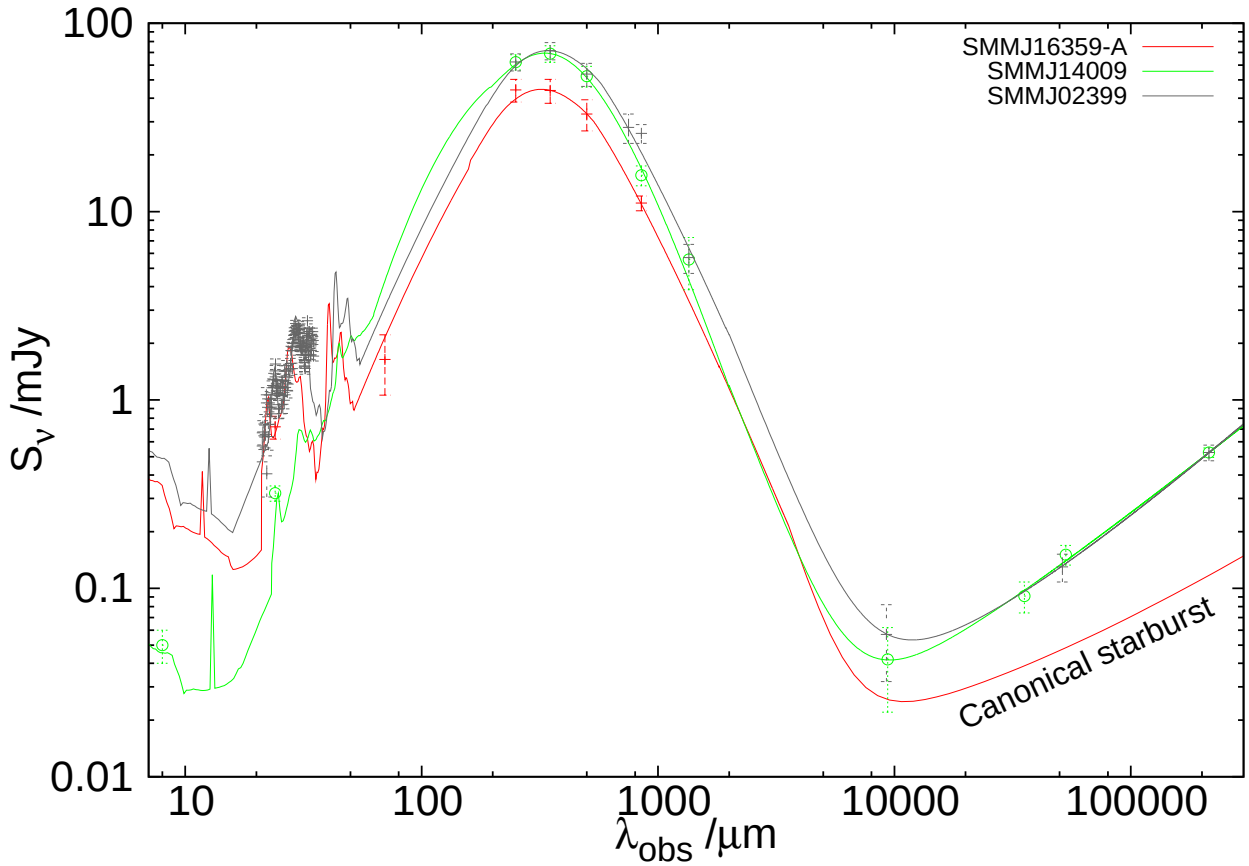

Figure 3. Observed-frame infrared SEDs for all of our sources, uncorrected for lensing, including data (*symbols: see legend*) and the corresponding best-fit CE01 SED. We include only data up to $\lambda_{obs} = 1350\,\mu$m in the fit. For clarity, we plot the SED of only one image of SMM J16359, and plot the best-fit CE01 template out to radio wavelengths, demonstrating the "canonical starburst" radio SED. For the other two galaxies, we truncate the CE01 SED at 2,000 μm and plot our modelled radio SED, constrained by our measurement of the Ka-band continuum flux and previously published results at longer wavelengths (§2.3, §3.5) and interpret the steepness of the resulting spectra as being consistent with the known AGN hosted within these galaxies.

Table 2. Observed properties.

Target	$z_{CO(1-0)}$	$I_{CO(1-0)}$ (Jy km s^{-1})	$I_{CO(3-2)}$ (Jy km s^{-1})	$r_{3-2/1-0}$	$\sigma_{CO(1-0)}$ (km s^{-1})	$\sigma_{CO(1-0)/CO(3-2)}$ (km s^{-1})	FWZI (km s^{-1})	R kpc
SMM J14009	2.9332 ± 0.0001	0.31 ± 0.02	2.70 ± 0.30	0.95 ± 0.12	175 ± 10	1.06 ± 0.08	850	1.2 ± 0.4
SMM J02399	2.8083 ± 0.0007	0.60 ± 0.12	3.10 ± 0.40	0.58 ± 0.14	350 ± 90	1.05 ± 0.26	1300	26 ± 4
SMM J16359-A	2.5174 ± 0.0002	0.22 ± 0.04	1.67 ± 0.13	0.83 ± 0.15	195 ± 15	1.10 ± 0.09	710	< 1
SMM J16359-B	2.5173 ± 0.0001	0.40 ± 0.04	2.50 ± 0.12	0.70 ± 0.22	190 ± 10	1.26 ± 0.07	780	0.6 ± 0.3
SMM J16359-C	2.5179 ± 0.0002	0.30 ± 0.09	1.58 ± 0.17	0.59 ± 0.20	305 ± 15	1.81 ± 0.09	670	4 ± 2

galaxies, SMM J14009 and SMM J02399, we detect velocity width ratios consistent with unity ($\sigma_{(1-0)/(3-2)} = 1.06 \pm 0.08$ and 1.05 ± 0.26 respectively).

3.2 Line luminosities and derived total gas masses

Traditionally, attempts to determine the molecular gas mass of distant galaxies via ^{12}CO emission have been subject to two main sources of uncertainty: (1) where mid-J lines are observed, a brightness temperature ratio, $r_{(3-2)/(1-0)} = 1$ has typically been assumed to convert the *measured* ^{12}CO $J = 3-2$ flux to an *inferred* $J = 1-0$ flux, and (2) the "X-factor", $X_{CO} = M(H_2)/L'_{CO(1-0)}$ (Downes & Solomon 1998) which is used to convert the observed or inferred ^{12}CO $J = 1-0$ luminosity to a total molecular gas mass. As a number of recent papers have shown (e.g. Harris et al. 2010; Ivison et al. 2011; Danielson et al. 2011, etc.), observed $r_{(3-2)/(1-0)}$ ratios in SMGs are typically well below unity. We can thus improve our gas mass estimates by observing the ^{12}CO line which traces the bulk of the molecular gas reservoir, but we must still worry about the order of magnitude range spanned by X_{CO} depending on the assumed state of the underlying ISM: $X_{CO} \sim 5$ in optically-thick giant molecular clouds (GMCs) where the gas is reducible to

Table 3. Lensing-corrected properties

Target	$L'_{\rm CO(1-0)}$ ($\times10^9$ K km s^{-1} pc^2)	$M_{\rm gas,\alpha}$ ($\times10^9$ M$_\odot$)	$m_{\rm CQ/SF}$	$L^a_{\rm IR}$ ($\times10^{11}$ L$_\odot$)	$M_{\rm gas,I11}$ ($\times10^9$ M$_\odot$)	$M_{\rm dyn}$ ($\times10^9$ M$_\odot$)
SMM J14009	83 ± 6	67 ± 4	0.09 ± 0.02	160 ± 16	35 ± 7	18 ± 4
SMM J02399	96.6 ± 1.9	77 ± 15	1.5 ± 0.5	81 ± 8	41 ± 14	1560 ± 550
SMM J16359-A	4.9 ± 0.8	3.9 ± 0.6	0.33 ± 0.09	7.1 ± 0.7	1.3 ± 0.4	< 19
SMM J16359-B	5.5 ± 0.6	4.4 ± 0.5	0.8 ± 0.3	6.2 ± 0.6	2.8 ± 1.3	11 ± 4
SMM J16359-C	10 ± 3	8 ± 2	1.4 ± 0.7	5.7 ± 0.6	1.5 ± 0.7	180 ± 70
A2218 #384	$3\sigma < 0.8$	$3\sigma < 0.6$	–	–	–	–

Note: [a]Calculations for $L_{\rm IR}$ discussed in §2.2. All luminosities have been corrected for the known magnification factors.

ensembles of self-gravitating units, whereas $X_{\rm CO} \sim 0.8$ in the more extreme environments of local ultra luminous infrared galaxies (ULIRGs), where the ISM forms a smooth, continuous medium. This latter value is typically adopted for SMGs.

The intrinsic ^{12}CO $J = 1-0$ line luminosity of an unlensed galaxy is the observed line flux integrated across the surface area and velocity range of the line: $L'_{\rm CO} = \int_{\Delta V} \int_{A_s} S_\nu \, dA \, dV$ K km s^{-1} pc^2, or:

$$L'_{\rm CO(1-0)} = 3.25 \times 10^7 \left[\frac{D_{\rm L}^2({\rm Mpc})}{1+z}\right] \left(\frac{\nu_{\rm rest}}{\rm GHz}\right)^{-2} \times \left[\frac{\int_{\Delta V} S_\nu d\nu}{\rm Jy\ km\ s^{-1}\ pc^2}\right] {\rm K\,km\,s^{-1}\,pc^2} \quad (1)$$

Having made an appropriate correction for magnification effects, we then invoke the commonly-used CO–H_2 gas mass conversion factor of Downes & Solomon (1998) of $X_{\rm CO} \sim 0.8\,{\rm M}_\odot\,({\rm K\,km\,s^{-1}\,pc^2})^{-1}$ to derive total gas masses (Table 3).

Combining our ^{12}CO $J=1$–0 data with existing $J=3$–2 data from Kneib et al. (2005, SMM J16359), Weiß et al. (2009, SMM J14009) and Genzel et al. (2003, SMM J02399) enables us to derive a mean magnification-weighted $T_{\rm b}$ ratio of $r_{(3-2)/(1-0)} = 0.72 \pm 0.12$ for the three images of SMM J16359, $r_{(3-2)/(1-0)} = 0.95 \pm 0.25$ for SMM J14009 and $r_{(3-2)/(1-0)} = 0.58 \pm 0.14$ for SMM J02399: SMGs on average experience *sub-thermal* excitation. We can then compare the gas mass derived above ($M_{\rm gas,\alpha}$) with a gas mass derived according to the prescription of Ivison et al. (2011), denoted $M_{\rm gas,I11}$, in which a lower limit for the mass of actively star-forming gas ($M_{\rm SF}$) is computed on the assumption that SMGs form stars at an appreciable fraction of Eddington-Limited star-formation efficiency ($\rm SFE_{max} = L_{IR}/M_{SF} \leqslant 500\,L_\odot\,M_\odot^{-1}$ where $L_{\rm IR}$ is the lensing-corrected infrared luminosity: Scoville 2004). For such maximally-efficient star formation, a measurement of $L_{\rm IR}$ therefore corresponds to a determination of $M_{\rm SF}$. Using canonical brightness temperature ratios for cold, quiescent ($r^{\rm (CQ)}_{(3-2)/(1-0)} = 0.3$) and warm, star-forming ($r^{\rm (SF)}_{(3-2)/(1-0)} = 1.0$) gas, their relative fractions in a sub-thermally-excited reservoir can be computed as

$$m_{\rm CQ/SF} = \frac{r^{\rm (SF)}_{(3-2)/(1-0)} - r_{(3-2)/(1-0)}}{r_{(3-2)/(1-0)} - r^{\rm (CQ)}_{(3-2)/(1-0)}} \quad (2)$$

and the total molecular gas mass is calculated as

$$M_{\rm gas} = M_{\rm SF}(1 + m_{\rm CQ/SF}) \quad (3)$$

Computing $M_{\rm gas}$ in this way provides an independent check on the total gas mass, based on different assumptions from those that underpin the X-factor method. The magnification-weighted mean value of $M_{\rm gas,I11}$ for SMM J16359 is $(2.1 \pm 0.6) \times 10^9$ M$_\odot$, and for SMM J02399 we detect $(41.0 \pm 14.4) \times 10^9$ M$_\odot$ of gas using this method. For SMM J14009 we calculate $M_{\rm gas,I11} = (34.9 \pm 7.3) \times 10^9$ M$_\odot$. All three values of $M_{\rm gas,I11}$ are $\sim 2\times$ lower than the equivalent values calculated via $X_{\rm CO}$, which would imply $X_{\rm CO} \sim 0.4$. We remind the reader, however, that $M_{\rm gas,I11}$ is calculated on the assumption that SMGs have maximal SFE: if the SFE is *less* than $500\,{\rm L}_\odot\,{\rm M}_\odot^{-1}$, then a higher mass of star-forming gas is required for a given $L_{\rm IR}$, raising the total gas mass in the system accordingly.

We can then compare these gas masses to the dynamical masses, assuming $M_{\rm dyn} = 2.1\,R\,\sigma^2_{\rm CO(1-0)}/G$ (Tacconi et al. 2008). Radii for our sources are derived by fitting a two-dimensional Gaussian to each integrated ^{12}CO $J=1$–0 map. This estimate assumes that the gas emission traces a virialised potential well. Using the observed values of $\sigma_{\rm CO(1-0)}$ reported in Table 2, we determine dynamical masses of $(18\pm4)\times10^9$ M$_\odot$, $(11\pm4)\times10^9$ M$_\odot$ and $(1560\pm550)\times10^9$ M$_\odot$ for SMM J14009, SMM J16359-B and SMM J02399, implying firm upper-limits of $X_{\rm CO} < 0.3$, $X_{\rm CO} < 2.8$ and $X_{\rm CO} < 24$, respectively. The dynamical masses derived from the two brighter images of SMM J16359 are $\sim 3\times$ higher than the best-estimate of the gas mass derived via $X_{\rm CO} = 0.8$, consistent with the sample of Ivison et al. (2011). The extremely compact radius quoted for SMM J14009 is a result of the narrowness of the 2D Gaussian that best fits the integrated map, itself a result of the source being only marginally resolved on North-South baselines and completely unresolved on East-West baselines. The gas in SMM J02399 was reported as having a lensing-corrected extent of $\sim$25 kpc in Ivison et al. (2010) in their C-configuration observations, corroborating the equally large extent of 26 ± 4 kpc derived from our D-configuration observations, as reported in Table 2. The colossal value of $M_{\rm dyn}$ therefore likely implies that the assumption the gas traces a virialised potential well is false.

3.3 Gas excitation: observed brightness temperature ratios

Having worked with canonical brightness temperature ratios to estimate $M_{\rm gas}$, free from any assumptions about $X_{\rm CO}$, we now compare our ^{12}CO $J=1-0$ spectra and the literature $J=3-2$ spectra in order to determine the true excitation conditions of the gas in our samples of galaxies.

The steepness of the observed radio continuum spectrum of SMM J02399 (§2.3) is consistent with the claim that this source harbours a powerful AGN. Such an AGN might be expected to heat the surrounding gas via bombardment with X-rays (Meijerink et al. 2006) or through shock-heating as the powerful radio jet drives into the surrounding molecular gas (Papadopoulos et al. 2011; Ivison et al. 2012), yet the $T_{\rm b}$ ratio detected for this source $r_{(3-2)/(1-0)} = 0.58 \pm 0.14$ is entirely consistent with that of less AGN-like SMGs. As Ivison et al. (2010) observe, however, SMM J02399 appears to consist of three or more interacting galaxies embedded within a larger reservoir of cold molecular gas. In particular, the massive obscured starburst which gives rise to the extreme $L_{\rm IR}$ of this source is spatially offset from the broad-absorption-line quasar.

Our improved sampling of the radio SED of SMM J14009 allows us to determine that this source also has a steep radio continuum spectrum (§2.3), corroborating its classification as an AGN. Additionally, SMM J14009 demonstrates a high $T_{\rm b}$ ratio, $r_{(3-2)/(1-0)} = 0.95 \pm 0.12$, which indicates the presence of a warm gas phase given the excitation requirements of the ^{12}CO $J = 3-2$ transition, $n_{\rm crit} \sim 10^4\,{\rm cm}^{-3}$, $E_{\rm u}/k_{\rm B} \sim 33\,{\rm K}$.

For SMM J16359, the magnification-weighted mean $T_{\rm b}$ ratio, $r_{(3-2)/(1-0)} = 0.72 \pm 0.12$, is entirely consistent with that of the SMG population (Harris et al. 2010; Ivison et al. 2011).

In addition to calculating source-averaged $T_{\rm b}$ ratios, our new data give us the spatial and spectral resolution to assess $r_{(3-2)/(1-0)}$ as functions of position and velocity. In Fig. 4 we illustrate the variation in gas excitation across the observed line profiles for the three sources. The results are only considered to be robust within the central $\pm 400\,{\rm km\,s^{-1}}$ of each of the line profiles due to deteriorating signal/noise at the edges of the line profiles; nevertheless, in SMM J16359 we see clear structure in the plot of $r_{(3-2)/(1-0)}$ versus velocity, with $r_{(3-2)/(1-0)} \sim 1$ for regions in the centre of the velocity-space, rolling off to sub-thermal values for the high-velocity wings of the line. These variations in the velocity fields of each galaxy may point to spatial variations in $r_{(3-2)/(1-0)}$, and are consistent with the observed values of $\sigma_{(3-2)/(1-0)}$.

We attempt investigate the velocity structure of our galaxies by constructing position-velocity (PV) diagrams for each source, extracting a slice through the (right-ascension, declination, velocity) data cube along the major axis of the galaxy. The resultant PV diagrams are shown in Fig. 5, however their low signal-to-noise prohibits us from modelling the emission.

3.4 Infrared-derived star-formation rates

We present our infrared SEDs in Fig. 3 and use the infrared luminosities reported in Table 3 with the truncation from Genzel et al. (2003) of the Kennicutt (1998, hereafter K98) conversion factor for a 1–100 $M_\odot$ Salpeter (1955) initial mass function (IMF) to compute ${\rm SFR_{IR}}$:

$$\frac{\rm SFR_{IR}}{1\ {\rm M_\odot yr^{-1}}} = \frac{L_{\rm IR}}{1.2 \times 10^{10}\,{\rm L_\odot}} \quad (4)$$

In the case of SMM J02399, $L_{\rm IR}$ is thought to arise roughly equally from the AGN and starburst components (e.g. Valiante et al. 2007). Adopting this AGN fraction for both SMM J02399 and SMM J14009, Equation 4 yields ${\rm SFR_{IR}} = 340 \pm 40$ and $670 \pm 70\,{\rm M_\odot\,yr^{-1}}$, respectively, where the uncertainties are purely statistical (due to $L_{\rm IR}$), and thus do not include the uncertainty in the K98 conversion factor.

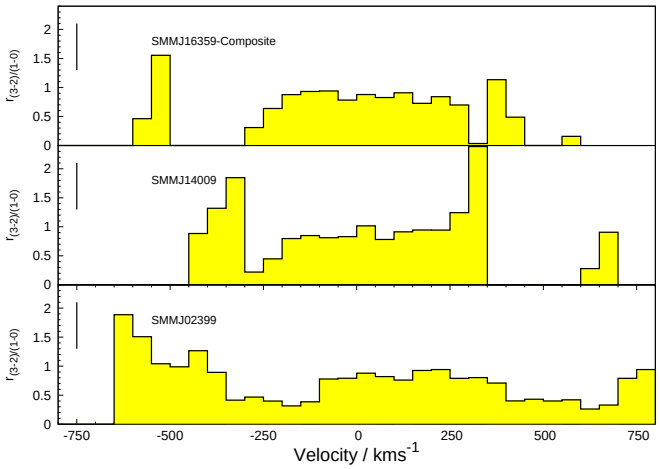

Figure 4. *Top – bottom:* Plots of $T_{\rm b}$ ratio as a function of velocity for the composite SMM J16359 spectrum, SMM J14009 and SMM J02399. Due to poor signal/noise at the extremities of the line profiles, we only consider data within the central $\pm 400\,{\rm km\,s^{-1}}$ to be robust enough to draw any conclusions from. The composite spectrum for SMM J16359 is computed by taking the magnification-weighted mean of the individual spectra from images A, B and C of this triply imaged source. The observed velocity offset between ^{12}CO $J = 1-0$ and $J = 3-2$ spectra in SMM J02399 manifests itself as a super-thermal $T_{\rm b}$ ratios in the envelope of the velocity profile. Typical uncertainties are denoted by the error bar in the top-left of each plot.

3.5 An independent probe of the SFR via optically-thin free-free emission

The SED longward of the FIR dust bump in galaxies is characterised by three main components: (i) the Rayleigh-Jeans tail of the infrared/sub-mm dust spectrum, (ii) thermalised free-free emission arising from ionised H II regions, which traces the massive/young stars ($> 5\,M_\odot$) capable of photoionising, and (iii) synchrotron radiation arising from the electrons accelerated by supernova remnants (Condon 1992, hereafter C92). Sometimes (iv) synchrotron radiation arising from plasma accelerated by an active AGN may also contribute.

Our data and the new estimates of $L_{\rm IR}$ provide us with the means to determine the SFR via two independent methods: (i) via $L_{\rm IR}$ between 1–100 $M_\odot\,{\rm yr^{-1}}$ (K98) and (ii) via the optically-thin free-free emission, probing ${\rm SFR}(\geqslant 5\,M_\odot)$ (C92).

We determine $\rm SFR_{radio}$ via Equation 5, where $L_{\rm ff}$ is the free-free luminosity density at frequency ν, defined such that $L = 4\pi d^2 S_{\rm ff}$ for lensing-corrected flux density, $S_{\rm ff}$. The free-free luminosity is derived by collating the radio continuum data summarised in Table 4, and fitting the relative contributions to the observed SED arising from dust (an extrapolation of the Rayleigh-Jeans side of the best-fitting CE01 infrared template), thermalised free-free emission ($S_{\rm ff} \propto \nu^{-0.1}$: C92) and synchrotron emission ($S_{\rm sync} \propto \nu^{-\alpha_{\rm sync}}$). The free

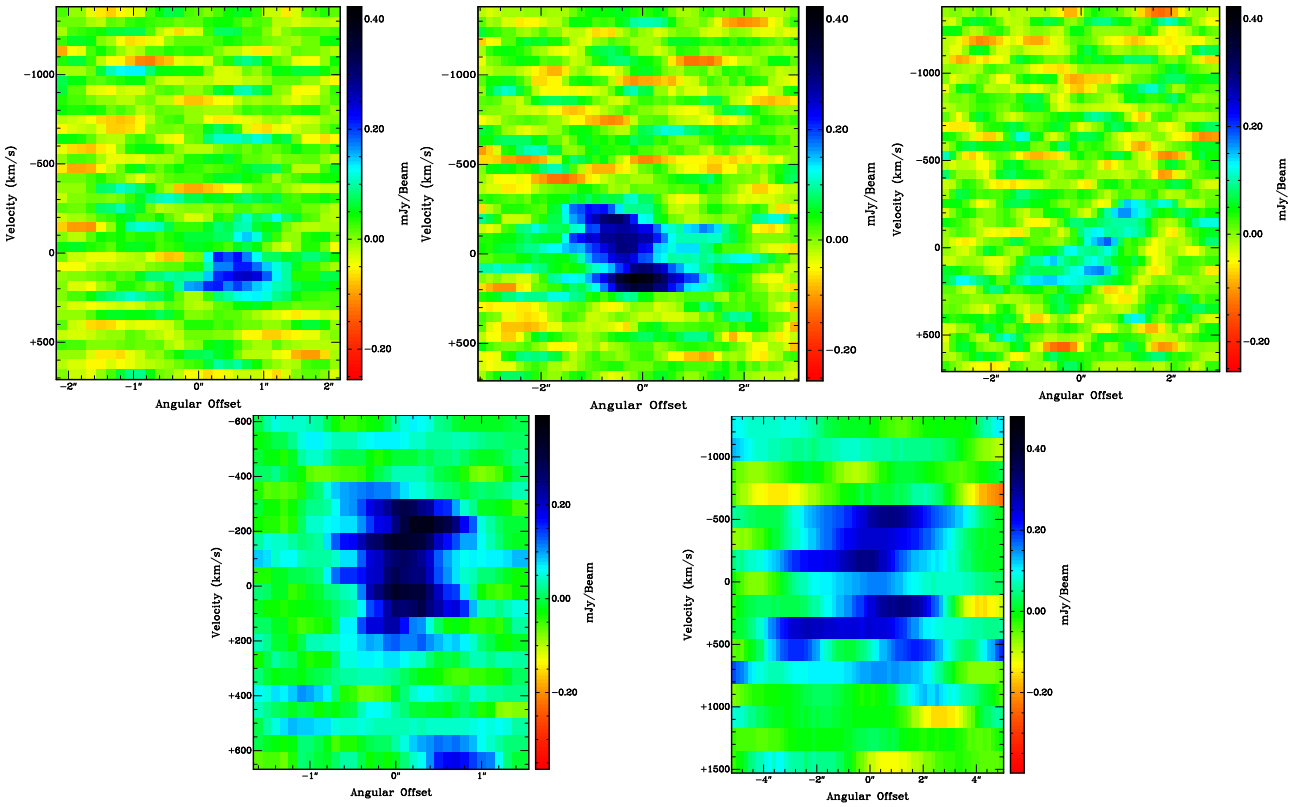

Figure 5. *Clockwise from top left:* Position-velocity diagrams for SMM J16359-A, SMM J16359-B, SMM J16359-C, SMM J02399 and SMM J14009.

parameters are the flux-scaling of the synchrotron and free-free emission, and also the spectral index, $\alpha_{\rm sync}$, of the synchrotron component.

$$\left(\frac{L_{\rm ff}}{\rm W\,Hz^{-1}}\right) \sim 5.5{\times}10^{20}\left(\frac{\nu}{\rm GHz}\right)^{-0.1}\left[\frac{\rm SFR(\mathit{M}\geqslant 5\,M_{\odot})}{\rm M_{\odot}yr^{-1}}\right] \quad (5)$$

Using the 1.4-, 5- and 8-GHz data available for our two galaxies, we measure spectral indices, α (where $S_\nu \propto \nu^\alpha$), of -0.96 ± 0.06 and -0.98 ± 0.14 for SMM J14009 and SMM J02399, respectively, a little steeper than the mean value of -0.75 ± 0.06 measured by Ibar et al. (2010) between 610 MHz and 1.4 GHz for 44 radio-detected SMGs in the Lockman Hole, and steeper too than the CE01 template that best fits each galaxy's mid-IR-to-submm SED.

The contributions to $S_{32\,\rm GHz}$ arising due to dust, synchrotron and free-free emission are presented in Table 5. We determine SFR($M \geqslant 5$ M$_\odot$) $= 290 \pm 85$ M$_\odot$ yr^{-1} for SMM J14009 and 200 ± 20 M$_\odot$ yr^{-1} for SMM J02399, and extrapolate down to 1 M$_\odot$. Accounting for the unseen low-mass stars using a Salpeter (1955) IMF, we find 1–100 M$_\odot$ SFR$_{\rm radio}$ of 630 ± 190 M$_\odot$ yr^{-1} and 430 ± 50 M$_\odot$ yr^{-1} for SMM J14009 and SMM J02399, respectively. In common with the preceding section, these uncertainties are statistical, and do not reflect the uncertainty in the C92 conversion factor.

3.6 The Lyman-break galaxy, Abell 2218 #384

Returning to the observations for SMM J16359, we searched for ^{12}CO $J = 1-0$ in the LBG at (R.A. 16:35:49.4, Dec. 66:13:07 J2000; Ebbels et al. 1996) located behind the same cluster. We do not detect this source, but set an upper limit using $S \leqslant 3\sigma_n\sqrt{\Delta v \Delta w}$ (Seaquist et al. 1995), where Δv is the velocity resolution of the spectrum, $\Delta w \sim 250\,{\rm km\,s^{-1}}$ is a typical LBG line width (Greve & Sommer-Larsen 2008) and the noise in the primary beam-corrected VLA spectrum is σ_n. We de-boost this by $\sim 16\times$ to account for gravitational lensing by the cluster (Ebbels et al. 1996) and thus derive upper limits on the ^{12}CO $J = 1-0$ luminosity of $< 0.8 \times 10^9$ Jy km s^{-1} pc^2 and on the gas mass of $< 6 \times 10^8$ M$_\odot$, respectively, where we have assumed $X_{\rm CO} = 0.8$, supposedly appropriate for star-forming galaxies.

This gas mass limit is comparable to gas masses detected in two similarly high-redshift LBGs by Riechers et al. (2010), who determined $M_{\rm gas} = (9.3 \pm 1.6) \times 10^8$ M$_\odot$ and $M_{\rm gas} = (4.6{\pm}1.1){\times}10^8$ M$_\odot$ for the same $X_{\rm CO}$, in the Cosmic Eye (at $z = 3.074$) and MS 1512-cB58 (at $z = 2.727$).

4 DISCUSSION AND CONCLUSIONS

4.1 The physical conditions of the molecular gas

We have presented high-resolution VLA imaging of ^{12}CO $J = 1-0$ in three bright, lensed SMGs. Two of our sources harbour known AGN – SMM J14009 and SMM J02399 – and are brighter ($L_{\rm IR} \sim 10^{13}$ L$_\odot$) than the unlensed sample of Ivison et al. (2011), while the other source – the triply imaged SMM J16359 – is an order of magnitude fainter ($L_{\rm IR} \sim 6 \times 10^{11}$ L$_\odot$, observed as being equally bright due to the high magnification afforded by its lensing cluster, Abell

Table 4. Observed radio properties

Target name	$S_{1.4\,\mathrm{GHz}}$ (μJy)	$S_{5\,\mathrm{GHz}}$ (μJy)	$S_{8\,\mathrm{GHz}}$ (μJy)	$S_{32\,\mathrm{GHz}}$ (μJy)	α
SMM J14009	$529^a \pm 30$	151 ± 17	91 ± 18	42 ± 20	0.96 ± 0.06
SMM J02399	$526^b \pm 50$	130 ± 22	N/A	57 ± 25	0.98 ± 0.14

Notes: [a]Ivison et al. (2000); [b]Ivison et al. (1998).

Table 5. Radio source derived properties

Target name	$S_{\mathrm{Ka,sync}}$ (μJy)	α_{sync}	$S_{\mathrm{Ka,dust}}$ (μJy)	$S_{\mathrm{Ka,ff}}$ (μJy)	$\mathrm{SFR}^a_{\mathrm{radio}}$ $\mathrm{M_\odot\,yr^{-1}}$	$\mathrm{SFR}^{a,b}_{\mathrm{IR}}$ $\mathrm{M_\odot\,yr^{-1}}$
SMM J14009	22 ± 2	1.01 ± 0.09	8 ± 1	12 ± 5	630 ± 190	670 ± 70
SMM J02399	16 ± 4	1.09 ± 0.13	18 ± 1	24 ± 6	430 ± 50	340 ± 40

Notes: [a]SFRs calculated for 1-100 $\mathrm{M_\odot}$ Salpeter IMF; [b]$\mathrm{SFR_{IR}}$ calculated on the assumption that the AGN and star formation contribute equally to L_{IR}.

2218), and does not appear to be dominated by AGN emission.

Comparing integrated maps of ^{12}CO $J=1$–0 and $J=3$–2 emission, we compute mean brightness temperature ratios of less than unity and velocity width ratios $\sigma_{(3-2)/(1-0)} \gtrsim 1$, both results consistent with the findings of Ivison et al. (2011): SMGs on average experience sub-thermal excitation and exhibit broad ^{12}CO $J=1-0$ line widths.

We derive L_{IR} for our galaxies by collating literature data, and then choosing from the SED library of Chary & Elbaz (2001) the best-fitting SED, which we integrate between rest-frame 8–1,000 μm. Next, we compute molecular gas masses via two methods: first by converting L'_{CO} to M_{gas} via an X-factor of $X_{\mathrm{CO}} = M(\mathrm{H_2})/L'_{\mathrm{CO}(1-0)}$ and then, as an independent check, using an approach that assumes SMGs form stars with Eddington-limited SFE, which gives us a lower-limit to the molecular gas mass. For each of our sources, the latter method yields a gas mass $\sim 2\times$ lower than that derived via X_{CO}.

4.2 Independent estimates of the SFR, and the role played by AGN

We compare SFRs derived via two independent diagnostics: (i) $\mathrm{SFR_{IR}}$, as computed via L_{IR} (K98) and (ii) $\mathrm{SFR_{radio}}$, computed from L_{ff}, the optically-thin free-free emission (C92) (Table 5). Both of these diagnostics are unaffected by interstellar extinction, however the former method is liable to over-estimate the SFR if a significant fraction of L_{IR} arises due to heating of dust by an AGN (Murphy et al. 2011). In contrast, the decomposition of the radio SED into dust, synchrotron and free-free contributions provides us with an SFR diagnostic that is directly related to the photoionisation rate of young, massive stars, relatively unaffected by AGN.

To derive $\mathrm{SFR_{IR}}$ in §3.4, we assumed that ∼50 per cent of L_{IR} was due to star formation, with the rest due to AGN heating of the dust (e.g. Frayer et al. 1998; Greve et al. 2005; Valiante et al. 2007). Here, we use our new measurements of free-free emission – which is unaffected by the presence of an AGN – to test this assumption. Using Equation 4 *without* an AGN correction, SMM J02399's $\mathrm{SFR_{IR,upper}}$ is $670 \pm 70\,\mathrm{M_\odot\,yr^{-1}}$. This is 35 ± 10 per cent higher than $\mathrm{SFR_{radio}}$ for a 1–100-$\mathrm{M_\odot}$ Salpeter IMF, implying a ∼35 per cent contribution to L_{IR} from its AGN. Similarly for SMM J14009, $\mathrm{SFR_{IR,upper}} = 1,340 \pm 140\,\mathrm{M_\odot\,yr^{-1}}$, indicating that some 55 ± 15 per cent of L_{IR} arises due to the AGN.

Recognising that the spatial extent traced by ^{12}CO $J=1-0$ for each of our galaxies is almost certainly larger than the region in which star formation is actively taking place, we can use our new free-free-derived SFRs to place lower-limits on the global star-formation rate surface density, $\Sigma_{\mathrm{SFR}} = 0.7 \pm 0.1\,\mathrm{M_\odot\,yr^{-1}\,kpc^{-2}}$ for SMM J02399 and $\Sigma_{\mathrm{SFR}} = 450 \pm 200\,\mathrm{M_\odot\,yr^{-1}\,kpc^{-2}}$ for SMM J14009, the former value again attributable to the colossal extent of the ^{12}CO $J=1-0$ reservoir in SMM J02399. We note that the peak Σ_{SFR} will be significantly higher than these galaxy-averaged values.

At present, our measurement of $\mathrm{SFR_{radio}}$ – and hence our estimates of the AGN fraction and Σ_{SFR} – are only as good as the extrapolation of the best-fit SED to the IR/submm data, via which we determine the dust contribution to the $\nu_{\mathrm{obs}} \sim 115$-GHz flux density, itself a relatively low signal-to-noise measurement. However, these uncertainties can be reduced significantly via better sampling of the SED beyond the wavelengths probed by *Herschel*. When complete, the VLA will offer 8 GHz of simultaneous bandwidth across 64 independently tunable sub-band pairs. Together with the Atacama Large Millimeter Array, it will be possible to measure the 350 μm–20 cm SEDs of these galaxies with an order of magnitude better sensitivity than currently possible.

ACKNOWLEDGEMENTS

We would like to express our immense gratitude to the VLA commissioning team and all those that have helped to create this remarkable facility. AT, IRS and RJI acknowledge support from STFC. IRS also acknowledges support from a Leverhulme Senior Fellowship. *Herschel* is an ESA space observatory with science instruments provided by European-led Principal Investigator consortia and with important participation from NASA. The National Radio Astronomy Observatory is a facility of the National Science Foundation

operated under cooperative agreement by Associated Universities, Inc.

REFERENCES

Bothwell M. S. et al., 2012, ArXiv e-prints
Brown R. L., Vanden Bout P. A., 1991, AJ, 102, 1956
Chapman S. C., Blain A. W., Smail I., Ivison R. J., 2005, ApJ, 622, 772
Chary R., Elbaz D., 2001, ApJ, 556, 562
Condon J. J., 1992, ARA&A, 30, 575
Danielson A. L. R. et al., 2011, MNRAS, 410, 1687
Downes D., Solomon P. M., 1998, ApJ, 507, 615
Ebbels T. M. D., Le Borgne J.-F., Pello R., Ellis R. S., Kneib J.-P., Smail I., Sanahuja B., 1996, MNRAS, 281, L75
Finkelstein K. D. et al., 2011, ApJ, 742, 108
Frayer D. T., Ivison R. J., Scoville N. Z., Yun M., Evans A. S., Smail I., Blain A. W., Kneib J.-P., 1998, ApJ, 506, L7
Genzel R., Baker A. J., Tacconi L. J., Lutz D., Cox P., Guilloteau S., Omont A., 2003, ApJ, 584, 633
Graham J. R., Liu M. C., 1995, ApJ, 449, L29
Greve T. R. et al., 2005, MNRAS, 359, 1165
Greve T. R., Sommer-Larsen J., 2008, A&A, 480, 335
Hainline L. J., Blain A. W., Smail I., Alexander D. M., Armus L., Chapman S. C., Ivison R. J., 2011, ApJ, 740, 96
Harris A. I., Baker A. J., Zonak S. G., Sharon C. E., Genzel R., Rauch K., Watts G., Creager R., 2010, ApJ, 723, 1139
Hempel A., Schaerer D., Egami E., Pelló R., Wise M., Richard J., Le Borgne J.-F., Kneib J.-P., 2008, A&A, 477, 55
Ibar E., Ivison R. J., Best P. N., Coppin K., Pope A., Smail I., Dunlop J. S., 2010, MNRAS, 401, L53
Ivison R. J., Papadopoulos P. P., Smail I., Greve T. R., Thomson A. P., Xilouris E. M., Chapman S. C., 2011, MNRAS, 412, 1913
Ivison R. J. et al., 2012, ArXiv e-prints
Ivison R. J., Smail I., Barger A. J., Kneib J.-P., Blain A. W., Owen F. N., Kerr T. H., Cowie L. L., 2000, MNRAS, 315, 209
Ivison R. J., Smail I., Le Borgne J.-F., Blain A. W., Kneib J.-P., Bezecourt J., Kerr T. H., Davies J. K., 1998, MNRAS, 298, 583
Ivison R. J., Smail I., Papadopoulos P. P., Wold I., Richard J., Swinbank A. M., Kneib J.-P., Owen F. N., 2010, MNRAS, 404, 198
Kennicutt R. C., Jr., 1998, ApJ, 498, 541
Kneib J.-P., 2010, in Macchetto F. D., ed, The Impact of HST on European Astronomy. Springer, p. 183
Kneib J.-P., Neri R., Smail I., Blain A., Sheth K., van der Werf P., Knudsen K. K., 2005, A&A, 434, 819
Kneib J.-P., van der Werf P. P., Kraiberg Knudsen K., Smail I., Blain A., Frayer D., Barnard V., Ivison R., 2004, MNRAS, 349, 1211
Lutz D., Valiante E., Sturm E., Genzel R., Tacconi L. J., Lehnert M. D., Sternberg A., Baker A. J., 2005, ApJ, 625, L83
Meijerink R., Spaans M., Israel F. P., 2006, ApJ, 650, L103
Morton D. C., Noreau L., 1994, ApJS, 95, 301
Murphy E. J. et al., 2011, ApJ, 737, 67
Negrello M. et al., 2010, Science, 330, 800
Papadopoulos P. P., Seaquist E. R., 1999, ApJ, 516, 114
Papadopoulos P. P., van der Werf P., Xilouris E. M., Isaak K. G., Gao Y., Muehle S., 2011, ArXiv e-prints
Pilbratt G. L. et al., 2010, A&A, 518, L1
Riechers D. A., Carilli C. L., Walter F., Momjian E., 2010, ApJ, 724, L153
Rowan-Robinson M. et al., 1991, Nature, 351, 719
Salpeter E. E., 1955, ApJ, 121, 161
Scoville N., 2004, in Astronomical Society of the Pacific Conference Series, Vol. 320, Aalto S., Huttemeister S., Pedlar A., eds, The Neutral ISM in Starburst Galaxies, p. 253
Seaquist E. R., Ivison R. J., Hall P. J., 1995, MNRAS, 276, 867
Smail I., Ivison R. J., Blain A. W., 1997, ApJ, 490, L5
Smail I., Ivison R. J., Blain A. W., Kneib J.-P., 2002, MNRAS, 331, 495
Solomon P. M., Radford S. J. E., Downes D., 1992, Nature, 356, 318
Tacconi L. J. et al., 2008, ApJ, 680, 246
Valiante E., Lutz D., Sturm E., Genzel R., Tacconi L. J., Lehnert M. D., Baker A. J., 2007, ApJ, 660, 1060
Weiß A., Downes D., Walter F., Henkel C., 2005, A&A, 440, L45
Weiß A., Ivison R. J., Downes D., Walter F., Cirasuolo M., Menten K. M., 2009, ApJ, 705, L45

This paper has been typeset from a TEX/ LATEX file prepared by the author.